
VERTICUE-BENCH: DIAGNOSING WHETHER MLLMs USE HEIGHT CUES TO RESOLVE 2D AMBIGUITY IN REMOTE SENSING NATURAL SCENES

Jing Huang^{1,*} Duanchu Wang^{2,*} Junjie Yang³ Zihang Cheng¹
 Cheng Li¹ Lin Cui¹ Zhouyi Wu¹ Di Wang^{1,†}

¹Xi'an Jiaotong University ²Xidian University ³University of Chinese Academy of Sciences

*Equal contribution †Corresponding author

ABSTRACT

Multimodal Large Language Models (MLLMs) have recently shown promising progress in geospatial reasoning. However, existing remote sensing benchmarks remain largely 2D-centric, evaluating models primarily on optical appearance. In natural environments, this paradigm breaks down due to severe spectral confusion, where ecologically distinct regions share similar textures but differ fundamentally in vertical structure. In such cases, explicit 3D structural data—such as Canopy Height Models (CHMs)—become essential geometric evidence for semantic disambiguation. Yet, it remains unclear whether current MLLMs can genuinely leverage vertical cues to resolve appearance-level ambiguity. To address this gap, we introduce VertiCue-Bench, the first diagnostic benchmark for CHM-grounded geospatial reasoning. VertiCue-Bench comprises 1,534 carefully curated instances across 17 tasks, explicitly disentangling low-level height perception from ambiguity-aware semantic reasoning. Evaluations on 14 state-of-the-art general and remote-sensing-specialized MLLMs, combined with counterfactual modality testing, reveal a striking perception–reasoning dissociation. While models exhibit emerging competence in reading raw CHM height cues, they largely fail to translate geometric perception into reliable semantic reasoning, often underperforming RGB-only baselines when joint constraints are required. Overall, VertiCue-Bench exposes a critical geometry-to-semantics gap in natural scene understanding, offering actionable insights for advancing geospatial MLLMs.

Keywords Remote Sensing · MLLMs · Canopy Height Models · Geometry-aware Reasoning

1 Introduction

Recent progress in multimodal large language models (MLLMs) has substantially expanded the scope of remote sensing tasks, ranging from general image understanding and question answering to complex geospatial grounding and large-scene reasoning [1, 2, 3, 4, 5, 6, 7, 8]. To evaluate these capabilities, a number of benchmarks have been proposed to test both general MLLMs and remote sensing-specific Vision-Language Models (RS-VLMs) [9, 10, 11, 12, 13, 14, 15, 16, 17, 18]. However, existing evaluations predominantly focus on 2D-related visual semantic tasks, mostly relying on optical imagery (e.g., RGB). Consequently, these benchmarks inherently evaluate models based on their ability to extract semantics from 2D appearance alone.

This 2D-centric evaluation paradigm faces a fundamental limitation in natural-scene remote sensing. In large-scale RGB orthophotos, ecologically distinct regions often exhibit highly similar 2D textures despite substantial differences in vertical structure—a phenomenon known as *spectral confusion* [19]. Dense shrubs, regenerating woodlands, and tall mature canopies, for example, may all present nearly identical green spectral patterns while differing markedly in vertical structures. As a result, distinctions that matter immensely for ecological analysis are often challenging to resolve reliably from RGB appearance alone.

In operational remote sensing workflows, human analysts routinely resolve this spectral ambiguity by consulting explicit 3D physical measurements [20, 21, 22]. When traditional 2D optical indices fail, experts rely on vertical information such as Canopy Height Models (CHMs), which provide spatially aligned height fields encoding physically meaningful canopy geometry [23, 24]. In this sense, the CHM is not merely an auxiliary modality, but a critical source of geometric evidence for resolving semantic bottlenecks. This raises an important question that remains insufficiently understood: *whether current MLLMs or RS-VLMs can genuinely use explicit geometric evidence, rather than relying primarily on RGB appearance, when appearance alone is not enough for correct judgment*. Existing geospatial MLLMs and benchmarks have made clear progress in perception and reasoning, but they still do not systematically test whether models can transform such CHM-provided vertical geometry cues into reasoning-ready evidence for semantic decisions under 2D ambiguity.

To bridge this evaluation gap, we introduce VertiCue-Bench, the first diagnostic benchmark for CHM-grounded geospatial reasoning. Rather than merely reporting coarse end-to-end scores, VertiCue-Bench systematically disentangles low-level height perception from ambiguity-aware downstream reasoning. Built on a specifically collected dataset, it comprises 1,534 standardized instances across 17 task types. This hierarchical framework evaluates models across multiple cognitive levels—spanning geometric reading, RGB-CHM cross-modal alignment, and semantic-geometric reasoning—to explicitly measure when, how and to what extent MLLMs utilize vertical structures.

Evaluating 14 MLLMs (including general and RS-specialize) on VertiCue-Bench reveals a pronounced perception-reasoning dissociation. Counterintuitively, while adding CHM consistently improves basic height perception, these gains fail to translate into reliable ambiguity-aware reasoning. In complex tasks requiring semantic-geometric fusion, performance often stagnates or even degrades compared to RGB-only inputs. This indicates that the primary bottleneck for current models is not extracting raw CHM signals, but rather converting these geometric cues into stable semantic decisions.

Overall, our contributions are as follows:

- We introduce VertiCue-Bench, a novel diagnostic benchmark specifically designed to evaluate whether MLLMs can use aligned geometry cues to resolve 2D ambiguity remote sensing natural scenes.
- We design a hierarchical evaluation framework that disentangles basic geometric perception from higher-order semantic-geometric reasoning.
- We uncover a critical geometry-to-semantics gap across 14 state-of-the-art MLLMs: while models demonstrate an emerging ability to perceive height cues, they fundamentally fail to integrate this geometric evidence for reliable semantic decision-making.

2 Related Work

2.1 Remote Sensing MLLMs and VLMs

The development of remote sensing vision-language models has roughly gone through three stages. Early studies [25, 26, 27] mainly focused on remote sensing vision-language representation learning and foundation model construction. However, their support for complex remote sensing tasks remained limited. Subsequent studies [1, 2, 3, 4, 28, 9, 29, 5] shifted toward adapting multimodal large models to remote sensing scenarios. However, they still mainly served semantic understanding and interactive analysis, with limited attention to deeper spatial cognition.

Recently, the field has moved beyond perception and question answering toward geospatial understanding and reasoning with higher cognitive complexity [30, 31, 7, 32, 6, 8]. GeoLLaVA-8K [30] improves modeling for ultra-high-resolution large-scene imagery, yet remains limited by sparse evidence acquisition. TerraMind [31] extends this line to generative multimodality for Earth observation, but does not explicitly focus on geometry-sensitive scene analysis. RSThinker [7] enhances faithful reasoning in remote sensing vision-language models, while leaving open how explicit geometric information should enter the reasoning process. Meanwhile, GeoEyes [32], GeoPixel [6], and RemoteReasoner [8] advance the field through visual focusing, fine-grained grounding, and unified reasoning workflows, respectively, but their results also suggest persistent limitations in evidence acquisition, spatial anchoring, and reasoning transfer.

Taken together, these studies have improved perception, grounding, and reasoning in different ways, yet they still fall short of establishing a stable transformation from geometric representations to semantic judgments, revealing an unresolved geometric-semantic gap in current remote sensing MLLMs.

2.2 Remote Sensing Benchmarks

Existing remote sensing multimodal benchmarks have broadly evolved from task-specific datasets to comprehensive evaluation frameworks. Early remote sensing multimodal benchmarks [9, 10, 11, 12] mainly focused on image captioning and visual question answering, with particular emphasis on assessing models’ ability to express scenes, attributes, counts, and simple relations in natural language. As the field has progressed, subsequent works [13, 14, 15, 16, 33, 34] have gradually moved beyond single-task settings toward unified and scenario-oriented evaluation, incorporating higher-level capabilities such as temporal change analysis and fine-grained recognition into broader benchmark frameworks. These developments have substantially advanced remote sensing vision-language research from closed-set recognition toward open-ended understanding and interaction. However, the evaluation paradigm of these benchmarks remains largely biased toward 2D visual semantics.

More recent studies have begun to explore more complex reasoning or 3D semantics [17, 18]. For example, VLRS-Bench [17] introduces complex reasoning in remote sensing into a systematic evaluation framework, emphasizing models’ cognitive, decision-making, and predictive abilities across multi-task scenarios. Geo3DVQA [18] constructs a height-aware question answering benchmark based on RGB aerial imagery to evaluate models’ ability to understand and reason about 3D attributes. Nevertheless, the former does not treat real height observations as mandatory evidence, while the latter mainly focuses on inferring 3D properties from RGB imagery, rather than evaluating whether models can truly perform semantic discrimination grounded in explicit height information.

To address this evaluation gap, we construct VertiCue-Bench, which treats CHM as explicit geometric evidence and investigates whether models can perform height-grounded semantic discrimination and geospatial reasoning when 2D appearance alone is insufficient to support reliable judgment.

3 VertiCue-Bench Design

This chapter introduces a hierarchical capability taxonomy for CHM cognitive diagnosis, details the benchmark construction pipeline, and summarizes the dataset statistics.

3.1 Hierarchical Capability Taxonomy

VertiCue-Bench organizes its evaluation hierarchy into a three-tiered capability framework (as shown in Figure 1): Layer 1 defines broad capability categories, distinguishing between perception and reasoning; Layer 2 adheres to a principle of progressive complexity, further refining these capabilities into five sequential levels; and Layer 3 maps each level to specific task-based capability points, thereby enabling a systematic assessment ranging from low-level geometric interpretation to high-level semantic-geometric fusion and reasoning. The detailed definitions are presented below.

3.1.1 Perception

Perception corresponds to Levels 1–4 (L1–L4) in the benchmark and is intended to evaluate whether a model can interpret the CHM as a geometric field with readable numerical values and spatial organization, without over-relying on high-level semantic priors. This capability domain starts from point-wise scalar reading and progressively extends to regional statistical reasoning, full-image structural analysis, and RGB–CHM cross-modal correspondence, thereby forming a hierarchical progression from local to global understanding and from unimodal to cross-modal perception.

- **L1 (Point Scalar Reading, PSR)** places little emphasis on semantic understanding and instead aims to isolate, to the greatest extent possible, the model’s basic ability to read and compare point-level height values. This level comprises four tasks: Height Classification (HC), Height Thresholding (HT), Relative Height Ranking (RHR), and Height Difference Classification (HDC).
- **L2 (Local Region Statistics, LRS)** extends the evaluation target from individual points to local regions of interest (ROIs), examining whether the model can extract statistical characteristics from intra-region height distributions and perform basic local geometric reasoning. Specifically, L2 consists of four leaf tasks: Central Tendency (CT), Threshold Coverage Estimation (TCE), Peak Localization (PL) and Stat Comparison (STC).
- **L3 (Global Structure Analysis, GSA)** further elevates the analysis scale to the entire image, focusing on the model’s ability to understand the global spatial structure of the CHM. Its tasks include Dominant Structure Localization (DSL), Trend Detection (TD), Global Structure Distribution (GSD).

VertiCue-Bench: Diagnosing Whether MLLMs Use Height Cues to Resolve 2D Ambiguity in Remote Sensing Natural Scenes

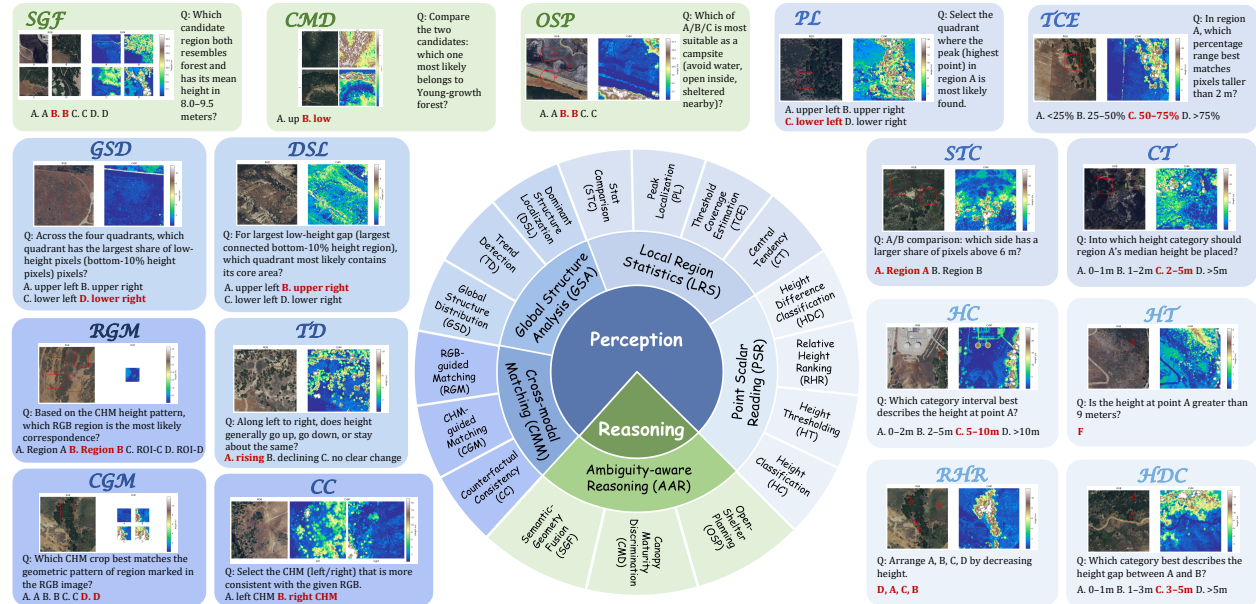


Figure 1: **Hierarchical capability taxonomy of VertiCue-Bench.** The benchmark is structured into two capability domains—Perception and Reasoning—spanning five levels from low-level CHM reading and RGB–CHM matching to ambiguity-aware semantic–geometric reasoning, with representative examples shown for each leaf task.

- **L4 (Cross-modal Matching, CMM)** aims to evaluate whether the model can establish stable and reliable cross-modal correspondences between RGB imagery and CHM. This level comprises three leaf tasks: RGB-guided Matching (RGM), CHM-guided Matching (CGM), and Counterfactual Consistency (CC).

3.1.2 Reasoning

Reasoning corresponds to L5 and is designed to evaluate whether a model can leverage the vertical structural cues provided by CHM to perform joint semantic–geometric reasoning when 2D appearance alone is ambiguous.

- **L5 (Ambiguity-aware Reasoning, AAR)** comprises three tasks: Semantic-Geometry Fusion (SGF), which focuses on region selection under joint semantic and height constraints; Canopy Maturity Discrimination (CMD), which requires distinguishing mature high-canopy forests from low shrubs or young stands with the aid of canopy height information; and Open-Shelter Planning (OSP), which involves site selection by jointly considering openness, water-body constraints, and surrounding shelter conditions. Accordingly, L5 moves beyond the reading and alignment of geometric information, and instead evaluates whether a model can genuinely transform CHM cues into a basis for semantic judgment and spatial decision-making in real-world scenarios characterized by 2D ambiguity.

3.2 Construction of VertiCue-Bench

As shown in Figure 2, the pipeline of VertiCue-Bench consists of three key stages: data source and preprocessing, automated ground-truth construction, and tuple generation. Its core objectives are twofold: to ensure strict alignment between RGB and CHM at the data level so that they can be jointly reasoned over, and to guarantee the objectivity, stability, and reproducibility of the benchmark at the annotation level through rule-based generation and manual quality inspection.

3.2.1 Data Source and Preprocessing

VertiCue-Bench is built upon the public Canopy height model and NAIP imagery pairs across CONUS dataset [35], which covers the conterminous United States and provides spatially matched CHM–NAIP pairs across diverse ecoregions and land-cover types. The source dataset was derived from USGS 3DEP airborne LiDAR and USDA NAIP aerial imagery, stratified by EPA Level III ecoregions and dominant NLCD land-cover classes, and was originally released for large-scale canopy height modeling. Each sample consists of a 1 m CHM chip and a time-aligned NAIP image

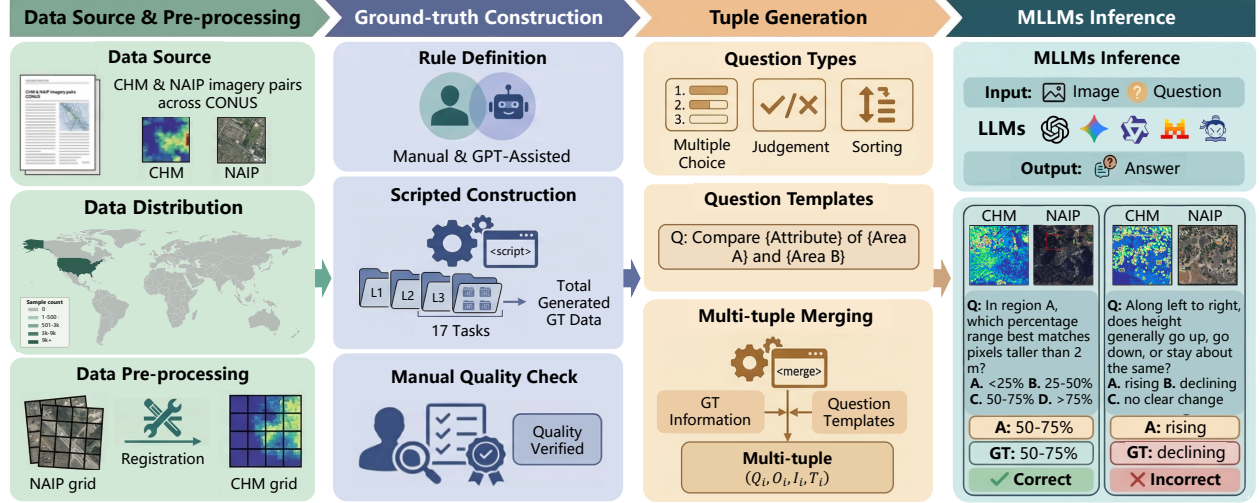


Figure 2: Overview of the construction pipeline of VertiCue-Bench.

with RGBN bands, whose native resolution varies from 0.3 m to 1.0 m. From this resource, we selected approximately 11,000 CHM–NAIP pairs as the raw data source. Since the source dataset provides spatially matched pairs with different native resolutions and pixel grids, the two modalities cannot be directly used for pixel-wise multimodal reasoning. We therefore performed a unified registration procedure before constructing the benchmark ground truth, ensuring that RGB semantics and CHM height cues are aligned at the pixel level for direct joint use.

3.2.2 Ground-truth construction

We construct the ground-truth (GT) through a three-step process: rule definition, scripted construction, and manual quality check. Mindful that automated annotation based on large language models may introduce additional biases [36], we strive to avoid involving GPT-class models deeply in core decision-making.

More specifically, the GT for L1–L3 is primarily derived through direct computation from CHM values on the unified grid. For these tasks, answers are determined automatically according to predefined numerical rules, together with anti-shortcut constraints that filter out samples solvable by trivial cues such as colorbar ranges, local extrema, or boundary conditions, thereby ensuring that models must genuinely perform geometric perception and comparison.

For L4, GT construction further shifts toward *cross-modal consistency assessment*. For L4-1 and L4-2, we define a unified matching score between a query patch and each candidate patch as:

$$S_{\text{total}} = \alpha_1 \cdot S_{\text{stats}} + \alpha_2 \cdot S_{\text{struct}} + \alpha_3 \cdot S_{\text{sal}}, \quad (1)$$

where S_{stats} , S_{struct} , and S_{sal} characterize matching consistency from the perspectives of global statistics, spatial structure, and salient structures, respectively. Since the first two constitute the primary sources of discriminative evidence, whereas the salient-structure term mainly serves an auxiliary role in distinguishing hard cases, we set $\alpha_1 = 0.4$, $\alpha_2 = 0.4$, and $\alpha_3 = 0.2$ in our experiments. The GT is determined by the candidate with the highest score, provided that the score margin is sufficiently large. For L4-3, we adopt a counterfactual CHM-swap mechanism. Under the constraint that the real and swapped CHMs remain close in global statistics, we quantify the spatial consistency between RGB and CHM using a multi-scale cross-modal alignment score. Let $G(R) = |\nabla \text{Gray}(R)|$ denote the gradient magnitude map of the grayscale RGB image. We then define

$$\text{align_score}(R, H) = \frac{1}{|S|} \sum_{s \in S} \rho(D_s(G(R)), D_s(H)), \quad (2)$$

where $S = \{4, 8, 16\}$ is the set of evaluation scales, $D_s(\cdot)$ denotes the downsampling operator at scale s , and $\rho(\cdot, \cdot)$ denotes the Spearman rank correlation. Only those samples are retained in which the true pairing consistently outperforms the substituted pairing at this score, thereby transforming the question of "whether CHM was genuinely utilized" into a diagnosable test of causal consistency.

L5 adopts a joint annotation framework of *semantic constraints–geometric thresholding–tolerance-aware filtering* to ensure that the GT can stably reflect the joint effect of semantic information and vertical structural information.

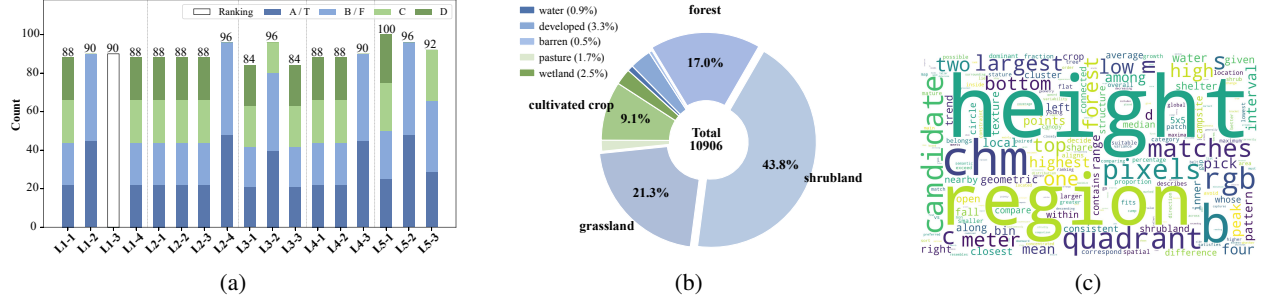


Figure 3: Overview of the dataset statistics. (a) Sample counts and answer distribution for each task. (b) Semantic category distribution. (c) Word cloud of the questions.

Specifically, we first construct sets of semantically consistent pixels based on the dominant land-cover types, and subsequently derive height information exclusively within the scope of these valid pixels; the extraction of pixels for each distinct semantic category is achieved through index-based constraints tailored to match their specific spectral characteristics. We then estimate the within-class height distributions over these semantically consistent pixels and fit a stable height range, $T_{\text{range}}(lc)$, for each category in an offline manner. During geometric decision making, instead of relying on a single hard threshold, we perform discrete sampling within $T_{\text{range}}(lc)$ and define

$$\text{geo_score} = \frac{1}{|T_{\text{set}}(lc)|} \sum_{t \in T_{\text{set}}(lc)} \mathbf{1}(\text{mean}_h > t) \quad (3)$$

to measure the stability with which a sample can be categorized as a high-structure or low-structure instance under the corresponding semantic class. Samples whose geo_score falls into the transition region between the high- and low-structure decision zones are treated as boundary-unstable and are therefore discarded.

Furthermore, to mitigate the sensitivity of the GT to parameter perturbations and incidental configurations within open-world scenarios, we have systematically incorporated robustness mechanisms—such as boundary buffering, constraint filtering, and stability verification—into the annotation process. This approach serves to filter out samples characterized by boundary instability or conditional fragility, thereby enhancing the robustness of the GT and reducing annotation ambiguity. Following the full-scale generation, we conduct further manual sampling for quality assurance to validate the quality of the constructed data.

3.2.3 Tuple generation

For each category of tasks, we have designed a distinct set of question templates—decoupled from the input modality and incorporating placeholders—thereby enabling a single task to naturally adapt to diverse input configurations. The question types consist of multiple-choice, true/false, and ranking questions, selected to facilitate quantitative evaluation. The script then automatically combines sample-level GT information with randomly selected templates to generate the final evaluation instances, which are uniformly represented as $P_i = (Q_i, O_i, I_i, T_i)$, where Q_i denotes the question, O_i denotes the set of candidate options, I_i denotes the set of input images, and T_i denotes the correct answer. This template-based generation approach not only ensures consistency in question intent and answers across different cross-modal settings but also provides a unified interface for subsequent input ablation studies, prompt control, and batch evaluation.

3.3 Dataset Statistics

VertiCue-Bench contains 1,534 standardized evaluation instances spanning 17 task types. As shown in Figure 3a, the sub-tasks are generally balanced in both sample size and answer distribution, which alleviates potential bias from label imbalance. As shown in Figure 3b and Figure 3c, the source data cover diverse land-cover semantics, while the question vocabulary simultaneously emphasizes geometric and semantic concepts such as height and forest. Together, these observations indicate that VertiCue-Bench is deliberately designed to probe the geometry–semantics gap in remote sensing, rather than focusing on pure geometric reading or isolated semantic recognition.

4 Experiments & Results

4.1 Experimental Setup

In our experiments, we evaluated 14 models on VertiCue-Bench, which can be grouped into three categories: 3 proprietary large VLMs, including GPT-5 [37], GPT-5-mini [37], Gemini-3-flash, 7 open-source VLMs: Qwen3.5 (9B) [38], Qwen3.5 (27B) [38], InternVL-3.5 (8B) [39], InternVL-3.5 (14B) [39], Mistral-Small-3.2 (24B) [40], Phi-4 (12B) [41], Gemma-3 (12B) [42], and 4 remote sensing specialized models: EarthDial [5], GeoChat [1], RemoteReasoner [8], RSThinker [7]. To ensure a fair and comparable evaluation across models, all VLMs were tested using the same zero-shot prompting strategy, with temperature set to 0, while keeping their default generation configurations unchanged. We use accuracy as the evaluation metric. For more details on experimental parameters, please see the appendix.

4.2 Experimental Protocols

We evaluate models on VertiCue-Bench under controlled input and inference settings to disentangle (i) the contribution of CHM, (ii) robustness to presentation variations, and (iii) the effect of external tools and privileged information.

- *Input modalities.* We consider two input modalities: **RGB-only**, where the model receives only the RGB visualization(s); and **RGB+CHM**, where the RGB visualization(s) are paired with the corresponding CHM visualization(s) as additional evidence. In this setting, the model is instructed to jointly use both modalities and treat CHM as complementary cues for vertical structure related patterns (see Appendix for details).
- *Primary benchmark setting.* Unless otherwise specified, we report results on the full VertiCue-Bench benchmark (1,534 instances across 17 tasks) under the **RGB+CHM** modality. All tasks are evaluated in a unified multiple-choice / true-false / ranking interface with identical scoring rules across settings.
- *Modality ablation.* To quantify the effect of CHM, we run a controlled comparison between **RGB-only** and **RGB+CHM** on tasks L1–L3 and L5. We exclude L4, whose cross-modal design intrinsically requires joint **RGB+CHM** input.
- *Robustness to presentation.* To test whether performance is sensitive to non-semantic presentation choices, we evaluate robustness under the **RGB+CHM** modality on a fixed subset of 496 samples while varying: (i) the order of prompts and images, (ii) image layout, (iii) color bar schemes, and (iv) numerical display settings. All other factors are held constant.
- *Inference settings: Raw, Tool, and Oracle.* We further study three inference conditions under the **RGB+CHM** modality on a subset of 380 samples: **Raw** (direct model prediction), **Tool** (model prediction with access to the specified tool outputs), and **Oracle** (prediction with privileged ground-truth cues), to isolate limitations from perception, tool use, and reasoning.
- *CHM counterfactual testing.* To verify whether models causally rely on CHM rather than spurious correlations, we conduct counterfactual tests for task L1 under the **RGB+CHM** modality on 133 samples. We compare **flip edits** (CHM edits designed to change the correct decision) against **placebo edits** (CHM edits that preserve the correct decision), while keeping RGB unchanged.
- *Error analysis.* Finally, we analyze error types and their distribution for task L5 based on the primary benchmark outputs to identify systematic failure modes.

4.3 Main Results

Table 1 summarizes the zero-shot performance of 14 MLLMs on VertiCue-Bench, revealing three key findings that expose a pronounced geometry-to-semantics gap in current models. Figure 4 provides representative examples of VertiCue-Bench evaluations.

Performance hierarchy. Table 1 shows a clear performance hierarchy across model families. Proprietary models achieve the strongest results on both Perception and Reasoning, open-source models form the middle tier, and remote-sensing-specialized models lag substantially behind. Notably, even the best specialized model, RemoteReasoner, reaches only 42.7% on L5 questions, far below leading generalist models such as GPT-5 (70.8%), GPT-5-mini (67.4%), Gemini-3-flash (66.2%), and Qwen3.5 (9B) (64.2%). This suggests that domain specialization in remote sensing does not automatically translate into stronger CHM-grounded reasoning.

Table 1: Main results on VertiCue-Bench across different model families.

Models	Perception					Reasoning			
	L1	L2	L3	L4	Overall	SGF	CMD	OSP	Overall
1. Proprietary Large Vision-Language Models									
GPT-5	48.9	65.0	41.7	58.6	54.1	48.0	80.2	<u>85.9</u>	70.8
GPT-5-mini	46.6	60.0	54.5	58.3	<u>54.7</u>	<u>42.0</u>	<u>76.0</u>	<u>85.9</u>	<u>67.4</u>
Gemini-3-flash	47.2	<u>64.4</u>	50.4	65.9	56.9	32.0	80.2	89.0	66.2
2. Open-Source Large Vision-Language Models									
Qwen3.5 (9B)	48.6	53.3	48.9	55.3	51.4	<u>42.0</u>	69.8	82.6	64.2
Qwen3.5 (27B)	50.3	55.8	<u>51.1</u>	<u>60.9</u>	54.3	39.0	74.0	77.2	62.8
InternVL-3.5 (8B)	26.7	35.8	32.2	37.2	32.7	37.0	55.2	62.0	51.0
InternVL-3.5 (14B)	34.6	44.7	34.1	36.8	37.9	<u>42.0</u>	62.5	58.1	54.2
Mistral-Small-3.2 (24B)	38.2	35.8	34.1	38.7	36.8	33.0	51.0	46.7	43.4
Phi-4 (12B)	25.6	26.4	16.3	31.2	25.0	25.0	42.7	35.9	34.4
Gemma-3 (12B)	32.9	36.7	28.4	38.3	34.2	28.0	51.0	56.5	44.8
3. Remote Sensing Specialized Models									
EarthDial	1.1	14.7	9.9	15.0	9.9	24.0	0.0	31.5	18.4
GeoChat	0.6	4.2	6.4	1.5	3.1	21.0	6.3	4.4	10.8
RemoteReasoner	32.6	33.6	26.9	27.8	30.7	39.0	54.2	34.8	42.7
RSThinker	24.9	33.3	25.0	33.5	29.2	18.0	46.9	23.9	29.5

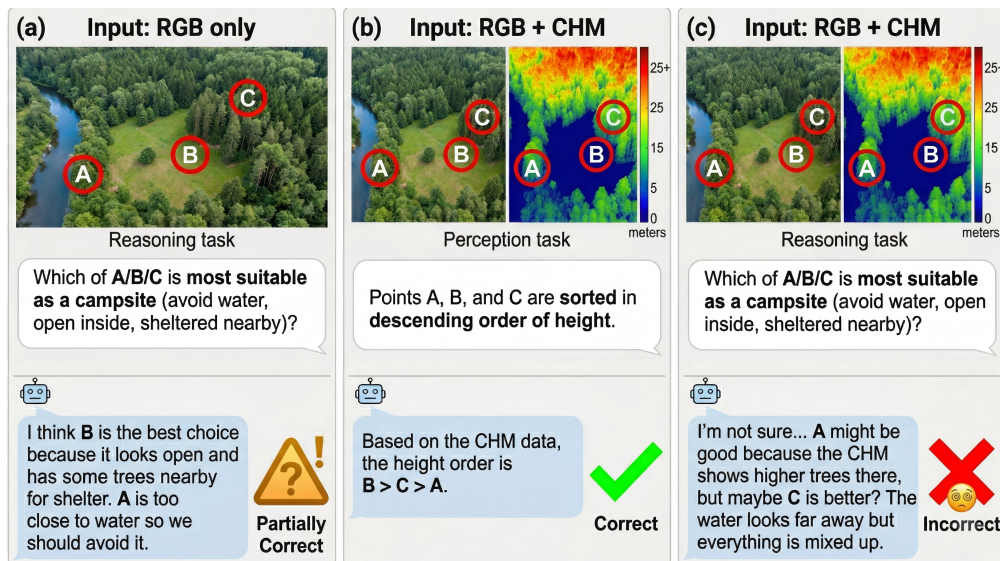


Figure 4: Examples of VertiCue-Bench evaluations.

Perception–reasoning gap. The most important signal in Table 1 is a clear dissociation between perceiving CHM cues and reasoning with them. Models that are better at low-level CHM perception do not necessarily achieve better downstream reasoning. For instance, Gemini-3-flash attains the highest Perception Overall (56.9%) but does not achieve the best Reasoning Overall, while scaling Qwen3.5 from 9B to 27B improves Perception (51.4% \rightarrow 54.3%) but slightly reduces Reasoning (64.2% \rightarrow 62.8%). This indicates that current MLLMs can increasingly read height information, yet still struggle to convert it into stable semantic-geometric decisions.

SGF as the main bottleneck. Within the 15 questions, the largest weakness consistently appears in Semantic-Geometry Fusion (SGF). Although many models score relatively high on CMD and OSP, the SGF remains much lower across the board. Since SGF requires jointly satisfying semantic and height constraints, this pattern suggests that the core limitation is not merely the perception of CHM signals, but the ability to bind geometric evidence with semantic understanding when resolving 2D ambiguity.

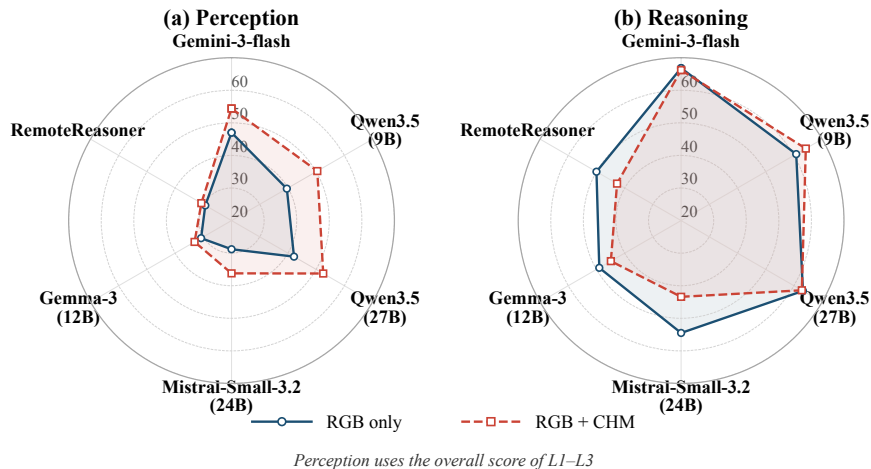


Figure 5: Perception-Reasoning Capability Comparison

Together, these results reveal a pronounced geometry-to-semantics gap in current MLLMs. Current models can often extract useful height cues from CHM, but they still fail to reliably use them for ambiguity-aware geospatial reasoning, which motivates deeper analyzes in the following ablation studies.

4.4 RGB-only vs. RGB+CHM

Figure 5 reveals a clear geometry-to-semantics gap in current MLLMs. While adding CHM consistently improves *Perception* by enabling models to extract height-related cues, it does not reliably enhance *Reasoning* over these cues. Across models, reasoning performance often remains unchanged, improves only marginally, or even degrades relative to RGB-only inputs. Even when gains are observed, they are typically much smaller than the corresponding improvements in perception.

This asymmetric pattern suggests that the main bottleneck is no longer simply whether models can read CHM, but whether they can transform CHM-derived evidence into stable semantic-geometric judgments for downstream decision-making. In other words, CHM already functions as a useful perceptual cue, but has not yet become reasoning-ready evidence for current MLLMs. The RGB-only versus RGB+CHM comparison therefore provides direct support for the geometry-to-semantics gap revealed by the main results.

4.5 Robustness to CHM Presentation

Table 2 examines the robustness of CHM gains under variations in input presentation and visual encoding. The results show that current MLLMs are far more sensitive to changes in presentation format than to perturbations in low-level visual encoding, suggesting that they still rely primarily on presentation-level alignment cues rather than learning robust, geometry-native cross-modal representations. Spatial co-registration emerges as the most critical factor affecting model performance. As shown in Table 2, separating RGB and CHM into multiple images substantially disrupts their explicit spatial correspondence and leads to severe information collapse. This indicates that current MLLMs still lack an effective ability to align spatial information across images. By contrast, changing the prompt order or colormap causes only minor performance fluctuations. Removing the colorbar results in a moderate drop, while using an incorrect colorbar is usually no more harmful than omitting it altogether. This suggests that models treat the colorbar mainly as a weak auxiliary cue rather than as a precise calibration reference.

4.6 Impacts of Inference Settings

Table 3 reports Raw, Tool, and Oracle setting results on a curated 380-sample subset of VertiCue-Bench for controlled diagnostic evaluation. Across models, performance improves substantially from the Raw to the Oracle setting, indicating that the main limitation does not stem from a lack of task-relevant information in CHM itself. Rather, current MLLMs struggle to convert raw CHM signals into reliable evidence for downstream reasoning. The Tool setting yields smaller and more model-dependent gains, suggesting that external CHM assistance is effective only when the host model can successfully interpret and integrate the returned evidence.

Table 2: Variant robustness under presentation and visual-encoding perturbations. The canonical baseline is *text-first + side-by-side composite + terrain + with colorbar*. Main values show absolute accuracy (%): superscripts indicate Δ Acc relative to the baseline. **Green** = gain, **red** = drop.

Model	Base Acc.	Presentation Variants		Encoding Variants				
		image-first	separate	viridis	gray	turbo	no colorbar	wrong colorbar
Gemini-3-flash	56.5	55.7 ^{-0.8}	28.6 ^{-27.9}	57.9 ^{+1.4}	54.2 ^{-2.3}	55.0 ^{-1.5}	53.6 ^{-2.9}	53.8 ^{-2.7}
Gemma-3 (12B)	35.7	32.7 ^{-3.0}	31.9 ^{-3.8}	32.3 ^{-3.4}	34.5 ^{-1.2}	34.3 ^{-1.4}	32.5 ^{-3.2}	33.3 ^{-2.4}
Mistral-Small-3.2 (24B)	35.3	34.3 ^{-1.0}	31.9 ^{-3.4}	36.1 ^{+0.8}	36.5 ^{+1.2}	34.9 ^{-0.4}	35.1 ^{-0.2}	35.3 ^{+0.0}
Qwen3.5 (9B)	50.8	51.8 ^{+1.0}	28.6 ^{-22.2}	50.0 ^{-0.8}	50.2 ^{-0.6}	49.8 ^{-1.0}	44.6 ^{-6.2}	50.4 ^{-0.4}
Qwen3.5 (27B)	53.8	52.3 ^{-1.5}	30.9 ^{-22.9}	51.3 ^{-2.5}	52.8 ^{-1.0}	51.6 ^{-2.2}	48.9 ^{-4.9}	49.4 ^{-4.4}
RemoteReasoner	29.8	32.7 ^{+2.9}	–	28.6 ^{-1.2}	32.5 ^{+2.7}	29.8 ^{+0.0}	28.8 ^{-1.0}	29.0 ^{-0.8}

Table 3: Raw, Tool, and Oracle setting evaluation on VertiCue-Bench.

Model	Setting	Accuracy (%)					Overall \uparrow	Δ
		L1	L2	L3	L4	L5		
Gemini-3-flash	Raw	44.0	60.0	77.5	65.0	58.3	58.4	–
	Tool	57.0	84.0	90.0	67.5	81.7	<u>73.7</u>	+15.3
	Oracle	100.0	99.0	85.0	63.7	<u>76.7</u>	86.8	+28.4
Qwen3.5 (9B)	Raw	50.0	60.0	65.0	58.8	63.3	58.2	–
	Tool	46.0	64.0	85.0	51.3	<u>75.0</u>	<u>60.5</u>	+2.3
	Oracle	100.0	98.0	82.5	56.3	80.0	85.3	+27.1
Qwen3.5 (27B)	Raw	52.0	56.0	77.5	62.5	65.0	60.0	–
	Tool	52.0	60.0	82.5	56.3	76.7	<u>62.1</u>	+2.1
	Oracle	100.0	98.0	85.0	68.8	<u>73.3</u>	87.1	+27.1
Mistral-3.2 (24B)	Raw	35.0	43.0	42.5	40.0	46.7	40.8	–
	Tool	42.0	49.0	55.0	33.8	<u>48.3</u>	<u>44.5</u>	+3.7
	Oracle	83.0	95.0	85.0	28.8	65.0	72.1	+31.3
Gemma-3 (12B)	Raw	37.0	38.0	42.5	38.8	40.0	38.7	–
	Tool	–	–	–	–	–	–	–
	Oracle	87.0	99.0	60.0	36.3	65.0	73.2	+34.5
RemoteReasoner	Raw	38.0	41.0	30.0	26.3	48.3	37.1	–
	Tool	–	–	–	–	–	–	–
	Oracle	80.0	76.0	37.5	25.0	55.0	59.0	+21.9

At the capability level, Oracle substantially improves L1–L3 for most models while providing only limited benefit on L4. This pattern suggests that making height information explicit can largely alleviate low-level CHM interpretation, but does not by itself resolve the RGB–CHM alignment challenge. Meanwhile, L5 improves consistently under Oracle and, for several models, also under Tool, indicating that downstream reasoning can benefit once geometric evidence is made more accessible and structured. Taken together, these results localize the primary bottleneck not to the absence of useful vertical cues, but to the models’ limited ability to access, align, and operationalize CHM evidence for semantic reasoning.

4.7 CHM Counterfactual Testing

As shown in Figure 6, all models exhibit a consistent pattern in which PSR remains close to the baseline while FSR is substantially lower. This suggests robustness to placebo edits that preserve the GT, but limited ability to update predictions when CHM edits genuinely change the correct answer. Consequently, irrelevant edits rarely disturb model outputs, whereas effective height-based interventions are not reliably translated into correct prediction updates.

Cross-model comparisons further reveal that sensitivity alone does not guarantee reliability. For instance, although gemma-3 achieves the highest FSR, its low baseline and PSR suggest unstable original decision-making. In contrast,

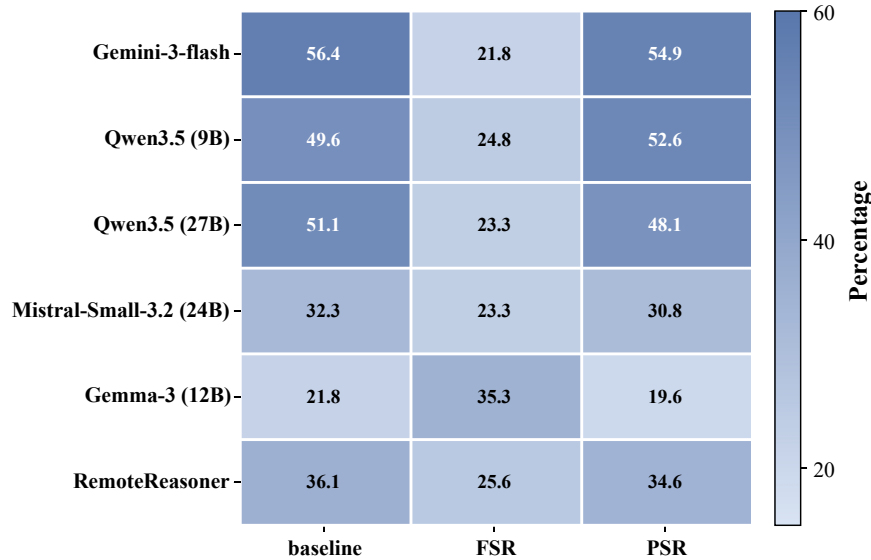


Figure 6: Results on CHM counterfactual testing. Flip Success Rate (FSR) and Placebo Stability Rate (PSR) is the proportion of flip-edit and placebo cases.

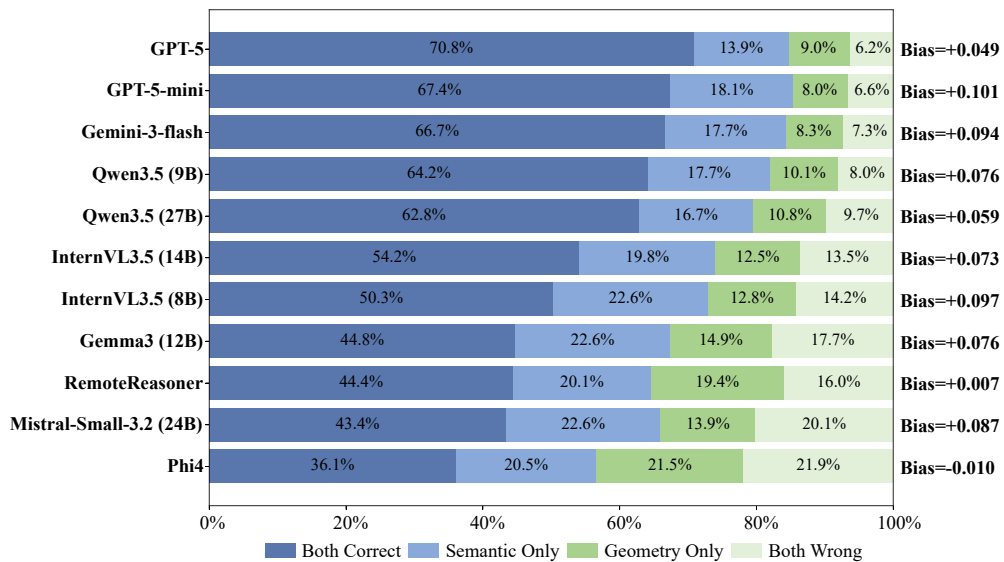


Figure 7: Error Decomposition

RemoteReasoner attains a relatively high FSR while maintaining a PSR close to its baseline, indicating improved sensitivity to CHM interventions without sacrificing robustness to irrelevant edits. Nevertheless, its overall accuracy still lags behind the strongest general-purpose models. Overall, the key challenge lies not in resisting placebo edits, but in consistently responding to effective CHM counterfactual changes.

4.8 Semantic Bias and Geometric Dependency

Figure 7 shows that *Semantic Only* exceeds *Geometry Only* in most cases on L5, indicating a systematic semantic bias when semantic and geometric cues conflict. Even for strong models such as GPT-5, higher accuracy mainly arises from aligned cues rather than consistent use of geometric constraints.

In contrast, the remote-sensing specialist model RemoteReasoner shows a more balanced error profile, with *Semantic Only* and *Geometry Only* being nearly comparable and the bias close to zero. This suggests that domain knowledge can improve sensitivity to CHM-based geometric cues. However, its *Both Correct* score still trails the strongest general-

purpose models, while its *Both Wrong* remains relatively high, indicating that domain priors alone are insufficient for semantic–geometric joint reasoning. Overall, the main bottleneck lies not in separately extracting semantic or geometric information, but in robustly integrating CHM evidence into reasoning under semantic conflict.

5 Conclusion

In this work, we introduced VertiCue-Bench, the first diagnostic benchmark designed to evaluate whether multimodal large language models can use canopy height models as explicit geometric evidence to resolve 2D ambiguity in remote sensing natural scenes. By organizing 1,534 instances across 17 tasks into a hierarchical framework spanning low-level perception, cross-modal matching, and ambiguity-aware reasoning, VertiCue-Bench enables a fine-grained diagnosis of how models read, align, and reason with height information. Extensive experiments on 14 MLLMs reveal a consistent geometry-to-semantic gap: although many models show emerging competence in perceiving CHM cues, these gains fail to translate into reliable semantic-geometric reasoning under ambiguous visual conditions. Our analyses further show that current models remain limited by weak RGB-CHM alignment, strong dependence on presentation format, and a persistent bias toward semantic appearance over geometric evidence. These findings suggest that the key challenge for future geospatial MLLMs is not simply accessing height information, but transforming geometric cues into reasoning-ready evidence for robust decision-making. We hope VertiCue-Bench can serve as a diagnostic testbed for developing models with stronger multimodal grounding, cross-modal alignment, and geometry-aware reasoning in remote sensing.

References

- [1] Kartik Kuckreja, Muhammad S. Danish, Muzammal Naseer, Abhijit Das, Salman Khan, and Fahad S. Khan. Geochat: Grounded large vision-language model for remote sensing. *The IEEE/CVF Conference on Computer Vision and Pattern Recognition*, 2024.
- [2] Dilxat Muhtar, Zhenshi Li, Feng Gu, Xueliang Zhang, and Pengfeng Xiao. Lhrs-bot: Empowering remote sensing with vgi-enhanced large multimodal language model. In *Computer Vision – ECCV 2024*, pages 440–457, Cham, 2025. Springer Nature Switzerland.
- [3] Yakoub Bazi, Laila Bashmal, Mohamad Mahmoud Al Rahhal, Riccardo Ricci, and Farid Melgani. Rs-llava: A large vision-language model for joint captioning and question answering in remote sensing imagery. *Remote Sensing*, 16(9), 2024.
- [4] Chao Pang, Xingxing Weng, Jiang Wu, Jiayu Li, Yi Liu, Jiaying Sun, Weijia Li, Shuai Wang, Litong Feng, Gui-Song Xia, and Conghui He. Vhm: Versatile and honest vision language model for remote sensing image analysis. *Proceedings of the AAAI Conference on Artificial Intelligence*, 39(6):6381–6388, Apr. 2025.
- [5] Sagar Soni, Akshay Dudhane, Hiyam Debary, Mustansar Fiaz, Muhammad Akhtar Munir, Muhammad Sohail Danish, Paolo Fraccaro, Campbell D Watson, Levente J Klein, Fahad Shahbaz Khan, et al. Earthdial: Turning multi-sensory earth observations to interactive dialogues. In *Proceedings of the Computer Vision and Pattern Recognition Conference*, pages 14303–14313, 2025.
- [6] Akashah Shabbir, Mohammed Zumri, Mohammed Bennamoun, Fahad Shahbaz Khan, and Salman Khan. Geopixel: Pixel grounding large multimodal model in remote sensing. In *Forty-second International Conference on Machine Learning*, 2025.
- [7] Jiaqi Liu, Lang Sun, Ronghao Fu, and Bo Yang. Towards faithful reasoning in remote sensing: A perceptually-grounded geospatial chain-of-thought for vision-language models. In *The Fourteenth International Conference on Learning Representations*, 2026.
- [8] Liang Yao, Fan Liu, Hongbo Lu, Chuanyi Zhang, Rui Min, Shengxiang Xu, Shimin Di, and Pai Peng. Remotereasoner: Towards unifying geospatial reasoning workflow. *Proceedings of the AAAI Conference on Artificial Intelligence*, 40(14):11883–11891, Mar. 2026.
- [9] Yuan Hu, Jianlong Yuan, Congcong Wen, Xiaonan Lu, Yu Liu, and Xiang Li. Rsgpt: A remote sensing vision language model and benchmark. *ISPRS Journal of Photogrammetry and Remote Sensing*, 224:272–286, 2025.
- [10] Kun Li, George Vosselman, and Michael Ying Yang. Hrvqa: A visual question answering benchmark for high-resolution aerial images. *ISPRS Journal of Photogrammetry and Remote Sensing*, 214:65–81, 2024.
- [11] Junjue Wang, Zhuo Zheng, Zihang Chen, Ailong Ma, and Yanfei Zhong. Earthvqa: Towards queryable earth via relational reasoning-based remote sensing visual question answering. In *Proceedings of the AAAI conference on artificial intelligence*, volume 38, pages 5481–5489, 2024.

- [12] Xing Zi, Jinghao Xiao, Yunxiao Shi, Xian Tao, Jun Li, Ali Braytee, and Mukesh Prasad. Rsvlm-qa: A benchmark dataset for remote sensing vision language model-based question answering. In *Proceedings of the 33rd ACM International Conference on Multimedia*, pages 12905–12911, 2025.
- [13] Xiang Li, Jian Ding, and Mohamed Elhoseiny. Vrsbench: A versatile vision-language benchmark dataset for remote sensing image understanding. *Advances in Neural Information Processing Systems*, 37:3229–3242, 2024.
- [14] Muhammad Danish, Muhammad Akhtar Munir, Syed Roshan Ali Shah, Kartik Kuckreja, Fahad Shahbaz Khan, Paolo Fraccaro, Alexandre Lacoste, and Salman Khan. Geobench-vlm: Benchmarking vision-language models for geospatial tasks. In *Proceedings of the IEEE/CVF International Conference on Computer Vision*, pages 7132–7142, 2025.
- [15] Xiao An, Jiaying Sun, Zihan Gui, and Wei He. CHOICE: Benchmarking the remote sensing capabilities of large vision-language models. In *The Thirty-ninth Annual Conference on Neural Information Processing Systems Datasets and Benchmarks Track*, 2025.
- [16] Fengxiang Wang, Hongzhen Wang, Zonghao Guo, Di Wang, Yulin Wang, Mingshuo Chen, Qiang Ma, Long Lan, Wenjing Yang, Jing Zhang, et al. Xlrs-bench: Could your multimodal llms understand extremely large ultra-high-resolution remote sensing imagery? In *Proceedings of the Computer Vision and Pattern Recognition Conference*, pages 14325–14336, 2025.
- [17] Zhiming Luo, Di Wang, Haonan Guo, Jing Zhang, and Bo Du. Vlrs-bench: A vision-language reasoning benchmark for remote sensing. *arXiv preprint arXiv:2602.07045*, 2026.
- [18] Mai Tsujimoto, Junjue Wang, Weihao Xuan, and Naoto Yokoya. Geo3dvqa: Evaluating vision-language models for 3d geospatial reasoning from aerial imagery. In *Proceedings of the IEEE/CVF Winter Conference on Applications of Computer Vision*, pages 4994–5003, 2026.
- [19] Dengsheng Lu and Qihao Weng. A survey of image classification methods and techniques for improving classification performance. *International journal of Remote sensing*, 28(5):823–870, 2007.
- [20] Mattia Balestra, Suzanne Marselis, Temuulen Tsagaan Sankey, Carlos Cabo, Xinlian Liang, Martin Mokroš, Xi Peng, Arunima Singh, Krzysztof Stereńczak, Cedric Vega, et al. Lidar data fusion to improve forest attribute estimates: A review. *Current Forestry Reports*, 10(4):281–297, 2024.
- [21] Jingru Wu, Qixia Man, Xinming Yang, Pinliang Dong, Xiaotong Ma, Chunhui Liu, and Changyin Han. Fine classification of urban tree species based on uav-based rgb imagery and lidar data. *Forests*, 15(2):390, 2024.
- [22] Ye Ma, Yuting Zhao, Jungho Im, Yinghui Zhao, and Zhen Zhen. A deep-learning-based tree species classification for natural secondary forests using unmanned aerial vehicle hyperspectral images and lidar. *Ecological Indicators*, 159:111608, 2024.
- [23] Yang Yao, Xiaoke Wang, Haiming Qin, Weimin Wang, and Weiqi Zhou. Mapping urban tree species by integrating canopy height model with multi-temporal sentinel-2 data. *Remote Sensing*, 17(5):790, 2025.
- [24] Yanshuang Wu and Xiaoli Zhang. Object-based tree species classification using airborne hyperspectral images and lidar data. *Forests*, 11(1):32, 2019.
- [25] Utkarsh Mall, Cheng Perng Phoo, Meilin Kelsey Liu, Carl Vondrick, Bharath Hariharan, and Kavita Bala. Remote sensing vision-language foundation models without annotations via ground remote alignment. In *ICLR*, 2024.
- [26] Fan Liu, DeLong Chen, Zhangqingyun Guan, Xiaocong Zhou, Jiale Zhu, Qiaolin Ye, Liyong Fu, and Jun Zhou. Remoteclip: A vision language foundation model for remote sensing. *IEEE Transactions on Geoscience and Remote Sensing*, 62:1–16, 2024.
- [27] Zilun Zhang, Tiancheng Zhao, Yulong Guo, and Jianwei Yin. Rs5m and georsclip: A large scale vision-language dataset and a large vision-language model for remote sensing. *IEEE Transactions on Geoscience and Remote Sensing*, pages 1–1, 2024.
- [28] Yang Zhan, Zhitong Xiong, and Yuan Yuan. Skyeyegpt: Unifying remote sensing vision-language tasks via instruction tuning with large language model. *ISPRS Journal of Photogrammetry and Remote Sensing*, 221:64–77, 2025.
- [29] Dilxat Muhtar, Zhenshi Li, Feng Gu, Xueliang Zhang, and Pengfeng Xiao. Lhrs-bot: Empowering remote sensing with vgi-enhanced large multimodal language model. In *Computer Vision – ECCV 2024*, pages 440–457, Cham, 2025. Springer Nature Switzerland.
- [30] Fengxiang Wang, Mingshuo Chen, Yueying Li, Di Wang, Haotian Wang, Zonghao Guo, Zefan Wang, Boqi Shan, Long Lan, Yulin Wang, et al. Geollava-8k: scaling remote-sensing multimodal large language models to 8k resolution. *arXiv preprint arXiv:2505.21375*, 2025.

- [31] Johannes Jakubik, Felix Yang, Benedikt Blumenstiel, Erik Scheurer, Rocco Sedona, Stefano Maurogiovanni, Jente Bosmans, Nikolaos Dionelis, Valerio Marsocci, Niklas Kopp, et al. Terramind: Large-scale generative multimodality for earth observation. In *Proceedings of the IEEE/CVF International Conference on Computer Vision*, pages 7383–7394, 2025.
- [32] Fengxiang Wang, Mingshuo Chen, Yueying Li, Yajie Yang, Yifan Zhang, Long Lan, Xue Yang, Hongda Sun, Yulin Wang, Di Wang, et al. Geoeyes: On-demand visual focusing for evidence-grounded understanding of ultra-high-resolution remote sensing imagery. *arXiv preprint arXiv:2602.14201*, 2026.
- [33] Ke Li, Fuyu Dong, Di Wang, Shaofeng Li, Quan Wang, Xinbo Gao, and Tat-Seng Chua. Show me what and where has changed? question answering and grounding for remote sensing change detection. *arXiv preprint arXiv:2410.23828*, 2024.
- [34] Qingmei Li, Yang Zhang, Zurong Mai, Yuhang Chen, Shuohong Lou, Henglian Huang, Jiarui Zhang, Zhiwei Zhang, Yibin Wen, Weijia Li, et al. Can large multimodal models understand agricultural scenes? benchmarking with agromind. *arXiv preprint arXiv:2505.12207*, 2025.
- [35] Brady W Allred, Sarah E McCord, and Scott L Morford. Canopy height model and naip imagery pairs across conus. *Scientific Data*, 12(1):322, 2025.
- [36] YiFan Zhang, Huanyu Zhang, Haochen Tian, Chaoyou Fu, Shuangqing Zhang, Junfei Wu, Feng Li, Kun Wang, Qingsong Wen, Zhang Zhang, Liang Wang, and Rong Jin. MME-realworld: Could your multimodal LLM challenge high-resolution real-world scenarios that are difficult for humans? In *The Thirteenth International Conference on Learning Representations*, 2025.
- [37] Aaditya Singh, Adam Fry, Adam Perelman, et al. Openai gpt-5 system card, 2025.
- [38] Qwen Team. Qwen3.5: Accelerating productivity with native multimodal agents, February 2026.
- [39] Weiyun Wang, Zhangwei Gao, Lixin Gu, et al. Internvl3.5: Advancing open-source multimodal models in versatility, reasoning, and efficiency, 2025.
- [40] Team MistralAI. Mistralai/mistral-small-3.1-24b-instruct-2503 · hugging face.
- [41] Marah Abdin, Jyoti Aneja, Harkirat Behl, et al. Phi-4 technical report, 2024.
- [42] Gemma Team, Aishwarya Kamath, Johan Ferret, et al. Gemma 3 technical report, 2025.